Infrared Physics & Technology xxx (2010) xxx–xxx

Contents lists available at ScienceDirect

Infrared Physics & Technology

journal homepage: www.elsevier.com/locate/infrared

Stability of widely tuneable, continuous wave external-cavity quantum cascade laser for absorption spectroscopy

Vasili L. Kasyutich [a,*], R.K. Raja Ibrahim [a,b], Philip A. Martin [a]

[a] School of Chemical Engineering and Analytical Science, University of Manchester, Manchester, M60 1QD, England, UK
[b] Universiti Teknologi Malaysia Skudai, 81310 Johor Bahru, Malaysia

ARTICLE INFO

Article history:
Received 7 January 2010
Available online xxxx

Keywords:
External-cavity quantum cascade laser
Mid-infrared absorption spectroscopy
Wavelength stability
Nitric oxide
Atmospheric pressure packed-bed plasma reactor
Allan variance plot

ABSTRACT

The performance of widely tuneable, continuous wave (cw) external-cavity quantum cascade laser (EC-QCL) has been evaluated for direct absorption spectroscopy measurements of nitric oxide (NO) in the wavenumber range 1872–1958 cm^{-1} and with a 13.5 cm long optical cell. In order to reduce the absorption measurement errors due to the large variations of laser intensity, normalisation with a reference channel was used. Wavelength stability within the scans was analysed using the Allan plot technique for the reduced wavenumber range of 1892.4–1914.5 cm^{-1}. The Allan variances of the NO absorption peak centres and areas were observed to increase with successive scan averaging for all absorption peaks across the wavelength scan, thus revealing short- and long-term drifts of the cw EC-QCL wavelength between successive scans. As an example application, the cw EC-QCL was used for NO measurements in the exhaust of an atmospheric pressure packed-bed plasma reactor applied to the decomposition of dichloromethane in waste gas streams. Etalon noise was reduced by subtracting a reference spectrum recorded when the plasma was off. The NO limit of detection (SNR = 1) was estimated to be ~2 ppm at atmospheric pressure in a 20.5 cm long optical cell with a double pass and a single 7 s scan over 1892.4–1914.5 cm^{-1}.

1. Introduction

Tuneable mid-infrared (mid-IR) single-frequency continuous wave (cw) external-cavity quantum cascade lasers (EC-QCL) have recently been introduced [1–3]. These can have wide wavelength tuning ranges of up to 182 cm^{-1} [1], narrow laser bandwidths of ~10–20 MHz [4,5] and cw output powers of up to 300 mW [6]. By comparison the typical tuning range of a cw distributed feedback (DFB) quantum cascade laser does not exceed 1–2 cm^{-1} by means of a current sweep and 10–12 cm^{-1} by laser temperature tuning from −25 °C to +50 °C. The application of a cw EC-QCL has been demonstrated in direct absorption spectroscopy [1], Faraday rotation spectroscopy of nitric oxide [7], quartz-enhanced photoacoustic absorption spectroscopy (QEPAS) [8], wavelength modulation spectroscopy of NO [1] and NO_2 [9], as well as in heterodyne detection [3,10]. Most of the work cited above has focused on measurements using in a narrow mode-hop-free scan of a few wavenumbers (2–4 cm^{-1}). However, tuneable broadband scanning mid-IR lasers are of interest for sensitive detection and measurements of multiple narrowband and broadband gaseous species [11,12] absorbing in a wide mid-IR spectral range up to a hundreds wavenumbers. The wide tuneability also enables their use in condensed phase measurements [13]. Currently Fourier transform infrared (FTIR) absorption spectrometers are primarily used for this, but are hampered by low intensity infrared light sources. The high power of the cw EC-QCL laser combined with a wide wavelength scan may allow faster temporal response and higher absorption sensitivity whilst using advanced laser based techniques such as wavelength/frequency modulation spectroscopy [14,15] as well as with high-finesse cavity-enhanced absorption spectroscopy [8,16]. From the limited number of publications it is unclear how well these novel cw EC-QCLs are suitable for such applications. For instance, high laser intensity variations were recently reported [5] and these variations within the broadband wavelength scan may obscure detection of small absorptions due to narrowband and broadband absorbers. A common approach to reducing the effects of laser intensity noise is to use balanced detection [17]. This is achieved by simultaneous recording of the intensities of a sample beam passed through an optical cell with an absorber and a reference beam produced from a beam splitter and passed outside the optical cell. Rationing the two beams produces a normalised spectrum with flatter baseline and reduced laser intensity noise. Unfortunately, an optical cell may also induce accidental etalon or interference fringe noise revealing in baseline variations of beam intensity drifting in time and during

* Corresponding author. Tel.: +44 161 306 8839; fax: +44 161 306 4399.
E-mail address: vasili.kasiutsich@manchester.ac.uk (V.L. Kasyutich).

1350-4495/$ - see front matter © 2010 Published by Elsevier B.V.
doi:10.1016/j.infrared.2010.07.004

wavelength tuning. Reduction, or full elimination, of etalons in the absorbance baseline can be achieved in principle by rationing a background spectrum produced by filling the cell with a buffer or scrubbed gas. However this approach relies on the assumption that changes between the sample and background spectra occur on longer timescales than the time to measure both spectra. This is often not the case and variations due to etalon effects, laser wavelength tuning linearity and the laser line width can vary on timescales sufficiently short to cause problems of measurement precision and accuracy. In order to obtain the best detection sensitivity one needs to select an appropriate approach for measurements and this depends upon the performance of the laser source.

Results obtained by direct absorption spectroscopy of nitric oxide (NO) are discussed for measurements in the exhaust of an atmospheric pressure packed-bed plasma reactor used for decomposition of dichloromethane (DCM) in waste gas streams. Non-thermal plasmas have been shown to have great potential for the decomposition of toxic volatile organic compounds (VOCs). An atmospheric pressure dielectric packed-bed plasma reactor can be used to decompose dichloromethane in a flowing gas mixture of nitrogen and oxygen [18]. Monitoring a wide variety of species such as N_2O, NO_2, CO_2, CO, $COCl_2$, CCl_4, HCl at the reactor exhaust after decomposition of DCM is typically based upon FTIR spectroscopy with a wavenumber range from 500–4000 cm^{-1}. Widely tunable cw EC-QCL based sources have the potential to provide multiple species detection with higher absorption sensitivity and faster time response in such studies.

In this paper the performance of a commercial cw EC-QCL for short-term and long-term wavelength stabilities has been evaluated using the Allan variance technique [19].

2. Experimental

The configuration of the mid-infrared laser spectrometer is shown in Fig. 1. A water-cooled cw EC-QCL head (model 21052-MHF, Daylight Solutions) and a tuneable QCL controller (model 1001TLC, Daylight Solutions) were used as a tunable single-frequency source of laser radiation with a tuning range of 1872–1958 cm^{-1} and an output power of less than 80 mW measured by means of a power meter (13 PEM001/J, CVI Melles Griot). The external-cavity of the laser was arranged with a diffraction grating in a Littrow configuration. As the grating angle and position were adjusted, the wavelength-dependent feedback into the gain medium was varied leading to wavelength tuneability across the entire gain band of the QCL and allowing for a tuneability of 10% to 25% of the centre wavelength. A beam splitter (8° wedge CaF_2 window) was used for splitting the laser beam into a sample beam and a reference beam. The sample beam passed through a 13.5 cm long optical cell formed by two flat KBr windows mounted at a small angle (~20°) on the facets of a 2.5 cm diameter Pyrex tube with two inlets for gas flow. The reference and sample beams were focused by two off-axis parabolic mirrors onto two thermoelectrically-cooled mercury cadmium telluride (MCT) photodetectors PD1 and PD2 (PVI-2TE-5, Vigo System S.A.), respectively. Both photodetectors' built-in preamplifiers (MIPDC-1.0, Vigo System S.A.) had a bandwidth of 1 MHz. The output of each photodetector preamplifier was sent to an 18 bit data acquisition board (USB-6281, 625 kS/s, National Instruments) with a sampling rate of 1 kHz under the control of a LabView program. A synchronisation "enable" signal from the laser controller was used to start recording the sample and reference traces, whilst the laser controller itself was run by means of commands transferred from the laptop via RS-232. The sample and the reference traces were then saved on a personal computer (PC) for further processing and analysis.

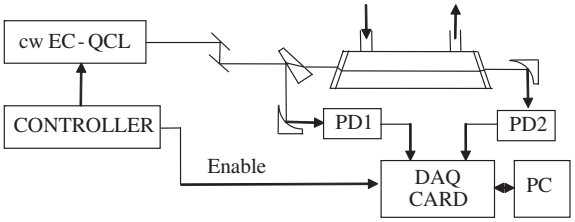

Fig. 1. Experimental setup of the mid-IR laser absorption spectrometer. cw EC-QCL is the continuous wave external-cavity quantum cascade laser. PD1 is the reference photodetector and PD2 is the sample photodetector.

2.1. Wavelength linearity

Typical output traces for the sample and reference beams are shown in Fig. 2. These were recorded for a NO flow ([NO] = 2700 ppm in nitrogen, flow rate of 14 cm^3/min, pressure of 760 Torr, temperature of 296 K). The absorptions in the reference beam are due to atmospheric water vapour in the laboratory atmosphere. Fig. 3a shows the resulting absorption spectrum between 1875 cm^{-1} and 1950 cm^{-1} calculated after normalisation of the sample trace by the reference trace at a time of 2.5 s. Fig. 3b shows the corresponding simulated absorption spectrum of NO (2700 ppm, a path length of 13.5 cm) and H_2O (0.96%, path length 26.5 cm) using the HITRAN database [20]. The absorption peak centre positions in the experimental and simulated spectra were extracted by use of a Matlab program. In total, 55 experimental points for peak centres were plotted against the simulated peak centre positions and these were fit by a straight line $A_1 + B_1 * X$, where $A_1 = -588$ s and $B_1 = 0.316$ s/cm^{-1} (see Fig. 4). The correlation coefficient was determined to be 0.99988, but the standard deviation of the experimental data from the fit was 0.1 s, which was equivalent to a wavenumber standard deviation of ~0.32 cm^{-1}. It is worth noting that the wavelength fit varies for successive scans. Such variations in the wavelength of the measured line centres demonstrate the necessity of accurate wavelength calibration for each wavelength scan.

2.2. Wavelength stability during successive scans

At room temperature, nitric oxide has two strong NO absorption doublets $R(6.5e)$ and $R(6.5f)$ at 1900.071 cm^{-1} and 1900.081 cm^{-1}, respectively, and an unresolved multiplet at ~1900.5175 cm^{-1} and so, depending on interfering species, this region is suitable for sensitive NO measurements. In order to estimate the wavelength sta-

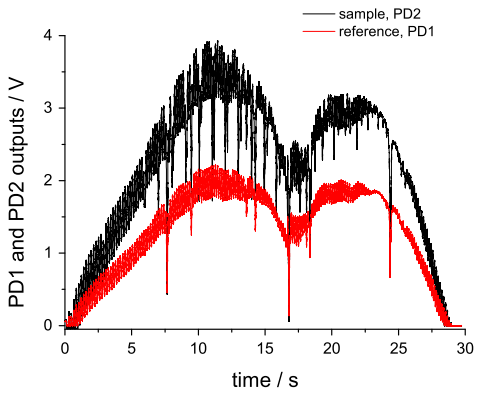

Fig. 2. Sample (PD2) and reference photodetector (PD1) output traces over the full range of the cw EC-QCL recorded for the cell with a 14 cm^3/min flow of NO (2700 ppm) in nitrogen at a pressure of 760 Torr, temperature of 296 K and a cell optical path length of 13.5 cm.

Please cite this article in press as: V.L. Kasyutich et al., Stability of widely tuneable, continuous wave external-cavity quantum cascade laser for absorption spectroscopy, Infrared Phys. Technol. (2010), doi:10.1016/j.infrared.2010.07.004

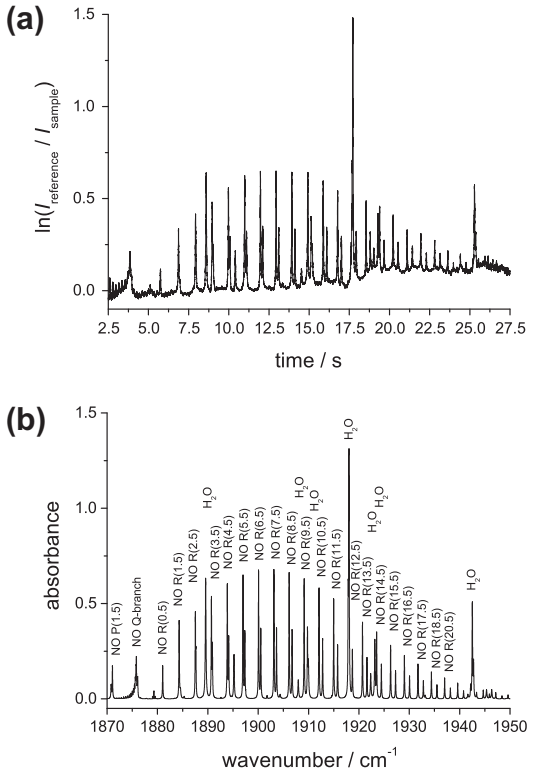

Fig. 3. Experimental (a) and simulated (b) absorption spectra for an NO concentration of 2700 ppm in nitrogen and ambient H_2O concentration of 0.96% at a pressure of 760 Torr, a temperature of 296 K and a cell optical path length of 13.5 cm.

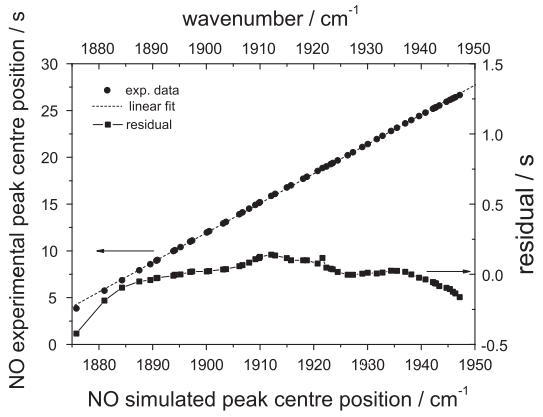

Fig. 4. A linear fit of the experimental absorption peak positions against those from the HITRAN simulated NO and H_2O absorption spectra. Shown also is the residual between the experimental data and the fit.

bility of the cw EC-QCL during successive scans, the tuning range was reduced to 1892.4–1914.5 cm^{-1}. The start of the data acquisition was synchronised from the leading edge of a trigger generated by the controller whilst a flow of NO in nitrogen passed through the cell at a rate of 14 cm^3 min^{-1}. The raw traces of the synchronisation signal, the sample and reference traces are shown in Fig. 5. The scan duration was 12 s and a total of 200 successive scans were saved for further analysis. As can be seen from Fig. 5, tuning from 1892.4 cm^{-1} up to 1914.5 cm^{-1} takes around 7 s, whereas reversing the grating to the initial position (see a reverse point on the Fig. 5) resulted in a return scan of duration around 5 s. In Fig. 5, only the first 10 s of each scan were recorded as the DAQ board

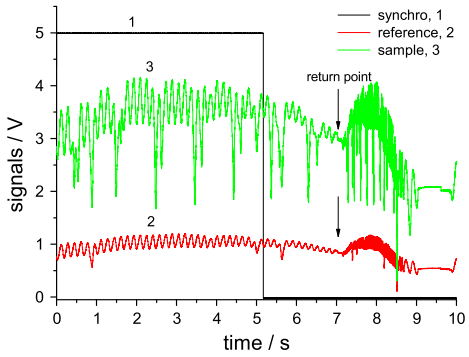

Fig. 5. Raw traces of synchronisation signal (black line 1), reference (red line 2) and sample (green line 3) outputs recorded by an 18 bit data acquisition board for a 2700 ppm NO in nitrogen flow through a 13.5 cm long cell at pressure of 760 Torr and temperature of 296 K. Traces between 10 and 12 s were not sampled and recorded. (For interpretation of the references to colour in this figure legend, the reader is referred to the web version of this article.)

was set to sample and record only 100,000 points after the level of the synchronisation signal from the EC-QCL rised above 2.5 V.

The absorption peak centre positions in the experimental and simulated spectra were extracted as described above. In total, fourteen experimental points for the peak centres were plotted against the simulated peak centre positions and these were fitted by a straight line $A_2 + B_2{*}X$, where $A_2 = -607$ s and $B_2 = 0.32$ s/cm^{-1}. The correlation coefficient was determined to be 0.99996, but the standard deviation of the experimental data from the fit was 0.019 s, which was equivalent to a wavenumber standard deviation of 0.06 cm^{-1} within the scan. The value of 0.06 cm^{-1} is by a factor of 5 less than the standard deviation of ~0.32 cm^{-1} observed for the wide 1875–1950 cm^{-1} scan.

A typical absorption spectrum of the narrower spectral region is shown in Fig. 6a, and a fit to the 5th and 6th absorption lineshapes with the fit residual is shown in Fig. 6b. In order to improve the precision of the lineshape fitting of the 5th and 6th peaks in Fig. 6b, the wavenumber conversion was carried out using the experimental peak positions of the 3rd, 4th, 5th, 6th, 7th and 8th lines. After this procedure, the two absorption peaks at 1900.1 cm^{-1} and 1900.6 cm^{-1} were fitted simultaneously by two Lorentzian lineshapes, whereas the etalon variation of the baseline was fitted by a product of a quadratic function and a sine function. The etalon variations of the baseline had a period of ~0.47 cm^{-1} and were assumed to be due to the etalons formed by the KBr flat windows on the sample cell. Rapid variations in the residual are clearly observed around the absorption peaks. These had an approximate spacing of ~0.016 cm^{-1}. This effect was not observed in a fit to the same absorption line under similar experimental conditions around 1900 cm^{-1} using a tuneable single-frequency cw DFB QCL [21,22]. It is thought that these variations in the fit residual observed with the cw EC-QCL could arise from the transient frequency jitter during wavelength tuning over the absorption lines. The frequency jitter is present across the whole scan but is only apparent for the stronger absorption lines where there is a larger variation of the intensity of the transmitted signal.

The peak centre positions of all fourteen absorption peaks were extracted for all 200 spectra recorded with 2700 ppm NO in nitrogen with a flow rate of 14 cm^3 min^{-1}, a pressure of 760 Torr and a gas flow temperature of 296 K. Fig. 7 shows the standard deviations of the peak centre positions in seconds and also in cm^{-1} after dividing the standard deviations by a factor of 0.32 s/cm^{-1} (an average for the B_2 coefficient for 200 scans). Larger standard deviations of the peak positions were observed towards the end of the scan.

Short-term and long-term stabilities of the cw EC-QCL wavelength within the scans were tested using the Allan variance tech-

Please cite this article in press as: V.L. Kasyutich et al., Stability of widely tuneable, continuous wave external-cavity quantum cascade laser for absorption spectroscopy, Infrared Phys. Technol. (2010), doi:10.1016/j.infrared.2010.07.004

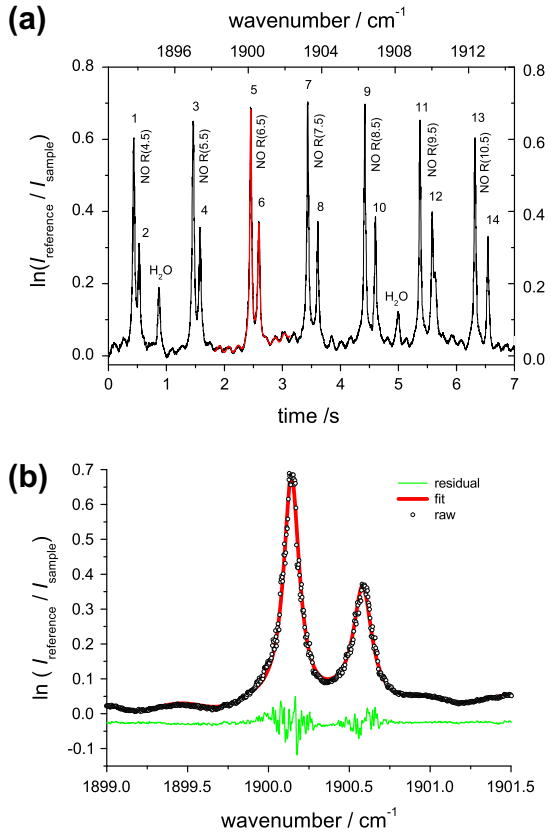

Fig. 6. Processed absorption spectra of NO (black line) and two Lorentzian lineshape fits to the experimental 5th and 6th absorption peaks for wide wavenumber scanning range (a) and selected and zoomed wavenumber range between 1899 cm^{-1} and 1901.5 cm^{-1} (b). The etalon variation of the baseline was fitted by a product of a quadratic function and a sine function. The signals were recorded for a 2700 ppm NO in nitrogen flow through a 13.5 cm long cell at pressure of 760 Torr and temperature of 296 K. For clarity the residual (green line) between the experimental and the fit on (b) is shifted down by 0.025. (For interpretation of the references to colour in this figure legend, the reader is referred to the web version of this article.)

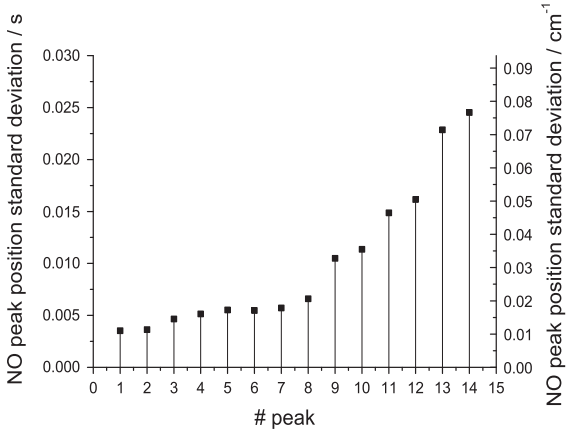

Fig. 7. Standard deviations of the 1–14th NO absorbance peak positions derived from 200 successive spectra with a 12 s individual time duration recorded at a 2700 ppm NO in nitrogen with a flow rate of 14 cm^3 min^{-1} at the pressure of 760 Torr and the gas flow temperature of 296 K.

nique [19]. The Allan variance can be described as a superposition of a simple power law drift noise with an arbitrary spectral exponent α and of a "white noise" ($\alpha = 0$) component for an integration time T [23,24]:

$$\sigma^2(T) = a/T + bT^{\alpha-1} \quad (1)$$

In most practical cases it is very useful to refer to the particular integration time corresponding to the minimum in the Allan variance plot [25,26]. This minimum describes the turn-over point where the "white" noise with a slope of "−1" in the logarithmic plot becomes dominated by the additional and undesired drift noise. Above the minimum time the root-mean-square of the measurements becomes much larger than is anticipated by the "white noise" equation alone. The Allan variance analysis was applied separately to the peak centre positions and also to the integrated absorbance areas. The variances were calculated for different numbers of successive scans (N) of the 200 recorded spectra using a program written in MathCad following an expression described elsewhere [14,26] for the strongest NO absorption peaks.

The Allan variances of the peak centre positions are shown in Fig. 8. It is instructive to consider three separate regions of the Allan variance plots. The first region of positive gradient (such as $1 \leqslant N \leqslant 6$), a second region where the variance decreases with increased averaging (such as $7 \leqslant N \leqslant 13$) and finally a region where the variance increases again with averaging (such as $N \geqslant 14$). A linear fit to the Allan variance in each of the three regions was performed and the slopes (β) are summarised in Table 1 for several absorption peaks. In the first region an increase in the Allan variance occurred for all the peaks across the spectrum slopes between 1.1 and 1.6. This can be explained by the dominance of short-term instrumental drifts of the actual EC-QCL laser wavelengths within each of the successive scans and giving a noise power spectrum of $1/f^{2.1}$–$1/f^{2.6}$. In the second region, the Allan variances were all observed to decrease to a minimum at around 12–14 successive scan averages or remain flat. In the third region the Allan variance was observed to increase again with successive scans in the average indicating a contribution from long-term wavelength drifts within the scan. The slope tends to increase across the scan so that peaks at the end of the scan (11 and 13) have a much higher increase in variance than those at the beginning of the scan. These longer-term instabilities of the EC-QCL wavelengths between the scans may limit the application of standard techniques used in absorption spectroscopy for improving the absorption sensitivity such as sweep averaging or subtraction of sample and "zero air" absorption spectra.

A similar analysis was carried out for the integrated absorbance areas rather than the peak positions. In this case it was applied only to the two strongest NO absorption lines in the region (the 3rd and 5th absorption peaks) for the same successively recorded 200 spectra. Fig. 9 shows the Allan variance plot for the two peak

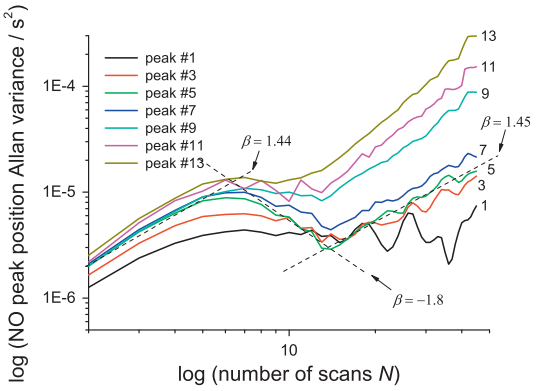

Fig. 8. The Allan variances of the absorption peak positions across the scan versus the number of scans included in each average (N). Also shown are linear fits (dashed lines) to the three regions of the Allan variance plot for the 5th NO R(6.5) absorption peak position at 2.465 s(1900.175 cm^{-1}).

Table 1
The slopes (β) of linear fits to the Allan variances of different NO absorption peak positions calculated for increasing number (N) of successive wavelength scans included in the average. The NO absorption peak assignment follows that shown in Fig. 6a.

NO peak/number of scan averages (N)	$1 \leqslant N \leqslant 6$	$7 \leqslant N \leqslant 13$	$N \geqslant 14$
Peak 1 at 0.630 s [1893.784 cm^{-1}]	1.14(0.07)	0(0.10)	0(0.1)
Peak 3 at 1.460 s [1897.048 cm^{-1}]	1.28(0.07)	−0.85(0.20)	1.15(0.05)
Peak 5 at 2.465 s [1900.175 cm^{-1}]	1.44(0.06)	−1.8(0.2)	1.45(0.04)
Peak 7 at 3.441 s [1903.260 cm^{-1}]	1.40(0.07)	−1.00(0.14)	1.42(0.03)
Peak 9 at 4.418 s [1906.344 cm^{-1}]	1.41(0.06)	−0.38(0.07)	1.94(0.04)
Peak 11 at 5.366 s [1909.340 cm^{-1}]	1.60(0.14)	−0.1(0.3)	2.17(0.04)
Peak 13 at 6.315 s [1912.335 cm^{-1}]	1.47(0.07)	0(0.17)	2.34(0.03)

areas. In the two plots a minimum in the variance cannot be discerned. The increase of the Allan variance indicates that the short- and long-term drifts of the laser wavelength, the laser intensity noise (due to etalon effects) and the transient laser frequency jitter appear to be the main contributors towards the errors in the NO integrated absorbance peak area measurements using broad wavelength scans of the cw EC-QCL. These results show that no amount of averaging will improve the error in the determination of the peak integrated absorbance.

2.3. NO measurements at the output of a plasma reactor

In order to evaluate the potential of the cw EC-QCL for studies of atmospheric pressure plasma reactors a longer optical cell with a base length of 20.5 cm and a double optical pass through the cell was arranged giving a total path length of 41 cm. Further details of the plasma reactor are given in reference [22]. The exhaust of the plasma reactor was first connected to a multipass cell (2.37 m) of an FTIR spectrometer (Bruker Equinox 55) by a 2 m long tube. The output of this cell was then connected to the EC-QCL cell by a 2.4 m tube. Thus, the plasma reactor, the FTIR cell and the cell used in the measurements with the EC-QCL were connected in series. Fig. 10 shows absorption spectra obtained by the EC-QCL spectrometer with the plasma switched on and off. The difference of the two spectra recorded is also shown in the Fig. 10 as a blue line shifted down for clarity. For the spectra recorded with the plasma on the oxygen concentration was 5%, the dichloromethane (DCM) concentration was ~500 ppm and nitrogen buffer gas was used with a total flow rate of 1 L/min. For the plasma off, the oxygen concentration was reduced to zero, the DCM concentration remained the same and the nitrogen buffer gas made up to a total flow rate of 1 L/min.

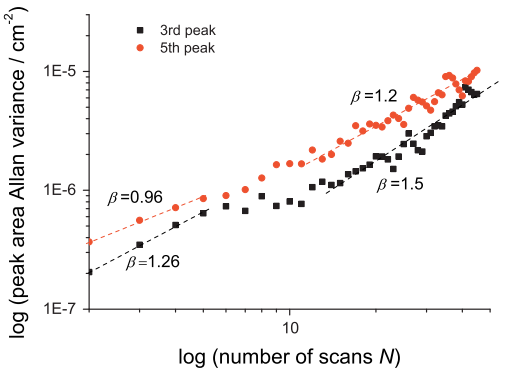

Fig. 9. The Allan variances of the integrated absorbance areas of the 3rd and 5th NO absorption peaks versus the average number of scans and their linear fits, where β refers to a slope of the linear fit.

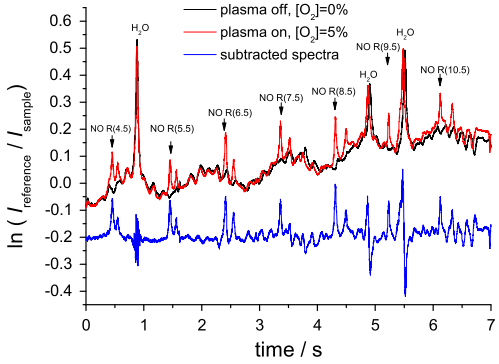

Fig. 10. NO absorption spectra recorded from the exhaust of a dielectric packed-bed plasma reactor. The two upper spectra (black and red) refer to the plasma with a DCM concentration of 500 ppm at the plasma rector inlet, a nitrogen buffer gas with total flow rate of 1 L/min and a pressure of 760 Torr. For the plasma "on" condition (red line), 5% O_2 was added to the inlet gas stream whereas for the plasma "off" condition (black line) the O_2 was removed. The spectra were recorded in an optical cell (total path length of 41 cm) which was connected via an FTIR optical cell to the exhaust of the plasma reactor. For clarity the subtracted NO absorption spectrum (blue line) is shifted down by 0.2. (For interpretation of the references to colour in this figure legend, the reader is referred to the web version of this article.)

Before subtraction the spectra were co-aligned along the wavenumber axis around the H_2O absorption peak at 1895.198 cm^{-1} (t = 0.88 s). This subtraction of the spectra was effective in the reduction of the etalon baseline noise only for the first half of the scans, whilst variations of the wavelength in the second part of the scans revealed themselves in the higher level of the etalon noise and in the derivative shape of the baseline around the strong absorption peaks. To obtain a better accuracy of the NO concentration measurements, the NO absorbance peaks at 1893.869 cm^{-1}, 1894.151 cm^{-1}, 1896.99 cm^{-1} and 1897.353 cm^{-1} were used for calculating the average NO concentrations at different oxygen concentrations. A typical processed NO absorption spectrum is shown in Fig. 11 at an oxygen concentration of 2%, DCM concentration of 500 ppm and nitrogen buffer gas at a flow rate of 1 L/min. The nitric oxide limit of detection (LOD) at SNR = 1 was estimated to be ~2 ppm at atmospheric pressure and a path length of 41 cm. Typical baseline standard deviations of around 0.001 were observed within these experiments at pressure of 760 Torr and temperature of 296 K.

Fig. 12 shows the variation in NO concentrations in the flow from the dielectric packed-bed plasma reactor at different oxygen concentrations in nitrogen and for an initial input of 500 ppm DCM. Previous measurements indicated that the deposited electri-

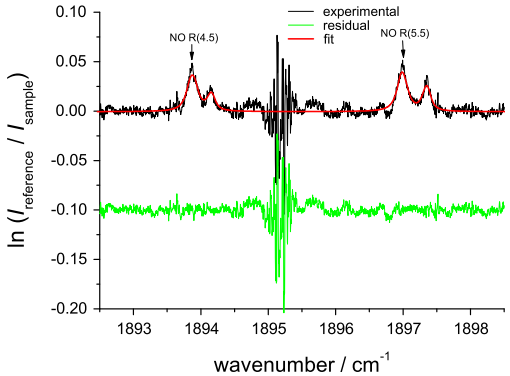

Fig. 11. Processed NO absorption spectra (black line), a fit (red trace) and a residual (green line) recorded for the packed-bed plasma reactor being switched on with 500 ppm DCM at the reactor inlet in a nitrogen buffer flow of 1 L/min, a pressure of 760 Torr and a temperature of 296 K. For clarity the residual is shifted down by 0.1. (For interpretation of the references to colour in this figure legend, the reader is referred to the web version of this article.)

Please cite this article in press as: V.L. Kasyutich et al., Stability of widely tuneable, continuous wave external-cavity quantum cascade laser for absorption spectroscopy, Infrared Phys. Technol. (2010), doi:10.1016/j.infrared.2010.07.004

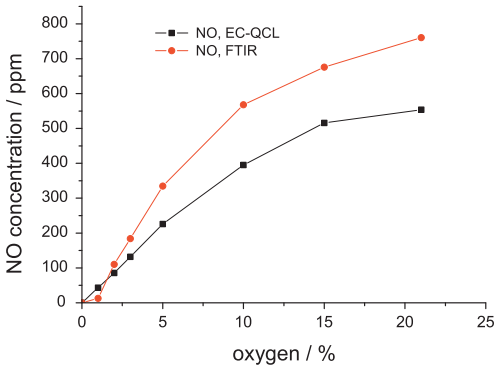

Fig. 12. NO concentration measurements using both FTIR (red line) and cw EC-QCL (black line) spectrometers as a function of added oxygen to the nitrogen flow with 500 ppm DCM to the dielectric packed-bed plasma reactor at the pressure of 760 Torr, total flow rate of 1 L/min and at plasma reactor power of 15 W. (For interpretation of the references to colour in this figure legend, the reader is referred to the web version of this article.)

cal power was about 15 W. NO measurements by means of the FTIR spectrometer connected directly to the output of the plasma reactor were slightly higher at high oxygen concentrations and this was explained by further oxidation reactions of NO in the 2.4 m long tube used to connect the FTIR multipass cell with the optical cell of the EC-QCL spectrometer. A NO LOD of 2 ppm in a 7 s single scan of 1892.4–1914.5 cm^{-1} is comparable to the LOD of 9 ppm achieved with single-frequency DFB QCL and averaging of 100 scans (1899.5–1901 cm^{-1}) within 0.1 s at atmospheric pressure in a 21 cm long optical cell [21]. It is worth noting that the NO LOD demonstrated here with a path length of 41 cm is markedly higher than the NO LOD of 0.7 ppbv (1 s observation time) and 1 ppbv (3 s averaging time) achieved by use of longer optical path lengths and a cw DFB QCL with a cavity-enhanced technique (high-finesse cavity with an effective path length of 700 m) [28] and wavelength modulation spectroscopy (a 76 m long multiple-pass optical cell) [30], respectively.

3. Discussion and conclusions

The performance of a tuneable cw EC-QCL was evaluated for direct absorption spectroscopy of nitric oxide. In order to reduce the effects of the large intensity variations (~15%) in the absorption measurements, normalisation of the sample trace to the reference trace was applied. From a linear fit of peak positions to HITRAN peak positions a typical standard deviation of 0.06 cm^{-1} was obtained for a narrow (1892.4–1914.5 cm^{-1}) single scan of the cw EC-QCL whereas this increased to 0.32 cm^{-1} for a wider (1875–1950 cm^{-1}) single scan. Typical baseline standard deviations of 0.0006–0.0015 were observed in the NO absorption spectra recorded within all experiments. Rapid larger variations in the residual between experimental data and a fit were clearly observed around the strong absorption peaks and were due to the transient frequency jitter within the wavelength tuning of the cw EC-QCL. This could be due to mechanical effects in the grating tuning mechanism.

For the narrower wavenumber tuning range of 1892.4–1914.5 cm^{-1} Allan variance analysis was applied to test the stability of wavelength tuning within successive scans. Short-term and long-term drifts were observed for all wavelengths during the scans, and this could limit further improvement of absorption sensitivity by the use of successive scan averaging of the low intensity beam at the output of long path length multiple-pass optical cells or high reflectivity mirror cavities in cavity-enhanced absorption spectroscopy. As an application the EC-QCL was applied to NO measurements produced in the decomposition of dichloromethane in an atmospheric pressure packed-bed plasma reactor. In order to reduce the effect of etalon noise, subtraction of a spectrum recorded with the plasma reactor being switched off was carried out. The nitric oxide limit of detection of about 2 ppm (SNR = 1) was routinely achieved with a 41 cm path length at atmospheric pressure. This was similar to that obtained with a cw DFB QCL laser. This LOD can be further improved with the high power of the EC-QCL using cavity-enhanced [27,28] and multiple-pass based techniques [29–31] for longer optical path length and single wavelength scan. For gas phase measurements, a wavelength calibration should be carried out simultaneously for each scan using a Fabry–Perot etalon and reference gas spectrum.

Acknowledgments

We thank Laser2000 UK for the loan of the EC-QCL. We would like to thank Ms Zaenab Abd Allah for help in use of a packed-bed plasma reactor. This work was conducted within the EPSRC project EP/G022933/1.

References

[1] G. Wysocki, R. Lewicki, R.F. Curl, F.K. Tittel, L. Diehl, F. Capasso, M. Troccoli, G. Hofler, D. Bour, S. Corzine, R. Maulini, M. Giovannini, J. Faist, Widely tunable mode-hop free external-cavity quantum cascade lasers for high resolution spectroscopy and chemical sensing, Appl. Phys. B 92 (2008) 305–311.
[2] E. Takeuchi, K. Thomas, T. Day, Applications multiply for external cavity QCL, Laser Focus World (January) (2009) 83–86.
[3] D. Stupar, J. Krieg, P. Krötz, G. Sonnabend, M. Sornig, T.F. Giesen, R. Schieder, Fully reflective external-cavity setup for quantum cascade lasers as a local oscillator in mid-infrared wavelength heterodyne spectroscopy, Appl. Opt. 47 (2008) 2993–2997.
[4] N. Mukherjee, R. Go, C.K.N. Patel, Linewidth measurement of external grating cavity quantum cascade laser using saturation spectroscopy, Appl. Phys. Lett. 92 (2008) 111116.
[5] G. Hancock, J.H. van Helden, R. Peverall, G.A.D. Ritchie, R.J. Walker, Direct and wavelength modulation spectroscopy using a cw external cavity quantum cascade laser, Appl. Phys. Lett. 94 (2009) 201110.
[6] R. Maulini, I. Dunayevskiy, A. Lyakh, A. Tsekoun, C.K.N. Patel, L. Diehl, C. Pflugl, F. Capasso, Widely tunable high-power external cavity quantum cascade laser operating in continuous-wave at room temperature, Electron. Lett. 45 (2009) 107–108.
[7] R. Lewicki, J.H. Doty III, R.F. Curl, F.K. Tittel, G. Wysocki, Ultrasensitive detection of nitric oxide at 5.33 μm by using external cavity quantum cascade laser-based Faraday rotation spectroscopy, Appl. Phys. Sci. 106 (2009) 12587–12592.
[8] A. Kosterev, G. Wysocki, Y. Bakhirkin, S. So, R. Lewicki, M. Fraser, F. Tittel, R.F. Curl, Application of quantum cascade lasers to trace gas analysis, Appl. Phys. B 90 (2008) 165–176.
[9] A. Karpf, G.N. Rao, Absorption and wavelength modulation spectroscopy of NO_2 using a tunable, external cavity continuous wave quantum cascade laser, Appl. Opt. 48 (2009) 408–413.
[10] D. Weidmann, G. Wysocki, High-resolution broadband (>100 cm^{-1}) infrared heterodyne spectro-radiometry using an external cavity quantum cascade laser, Opt. Express 17 (2009) 248–259.
[11] C. Young, S.S. Kim, Y. Luzinova, M. Weida, D. Arnone, E. Takeuchi, T. Day, B. Mizaikoff, External cavity widely tunable quantum cascade laser based hollow waveguide gas sensors for multianalyte detection, Sens. Actuators B 140 (2009) 24–28.
[12] M.C. Phillips, T.L. Myers, M.D. Wojcik, B.D. Cannon, M.S. Taubman, D.C. Scott, Measurement of broad absorption features using a tunable external cavity quantum cascade laser, Proc. SPIE 6760 (2007) 676003.
[13] J.A. Calladine, M.W. George, Studying highly reactive organometallic complexes with fast time-resolved infrared spectroscopy using external cavity quantum cascade lasers, Spectrosc. Eur. 21 (2009) 6–9.
[14] P. Werle, R. Miicke, F. Slemr, The limits of signal averaging in atmospheric trace-gas monitoring by tunable diode-laser absorption spectroscopy (TDLAS), Appl. Phys. B 57 (1993) 131–139.
[15] P.A. Martin, Near-infrared diode laser spectroscopy in chemical process and environmental air monitoring, Chem. Soc. Rev. 31 (2002) 201–210.
[16] S. Welzel, G. Lombardi, P.B. Davies, R. Engeln, D.C. Schram, J. Röpcke, Trace gas measurements using optically resonant cavities and quantum cascade lasers operating at room temperature, J. Appl. Phys. 104 (2008) 093115.
[17] D.D. Nelson, J.B. McManus, S.C. Herndon, M.S. Zahniser, B. Tuzson, L. Emmenegger, New method for isotopic ratio measurements of atmospheric carbon dioxide using a 4.3 μm pulsed quantum cascade laser, Appl. Phys. B 90 (2008) 301–309.

[18] Z. Abd Allah, D. Sawtell, V.L. Kasyutich, P.A. Martin, FTI and QCL diagnostics of the decomposition of volatile organic compounds in an atmospheric pressure dielectric packed bed plasma reactor, J. Phys. Conf. Ser. 157 (2009) 012001.
[19] D.W. Allan, Statistics of atomic frequency standards, Proc. IEEE 54 (1966) 221–230.
[20] L.S. Rothman, D. Jacquemart, A. Barbe, D.C. Benner, M. Birk, L.R. Brown, M.R. Carleer, C. Chackerian, K. Chance, L.H. Coudert, V. Dana, V.M. Devi, J.M. Flaud, R.R. Gamache, A. Goldman, J.M. Hartmann, K.W. Jucks, A.G. Maki, J.Y. Mandin, S.T. Massie, J. Orphal, A. Perrin, C.P. Rinsland, M.A.H. Smith, J. Tennyson, R.N. Tolchenov, R.A. Toth, J.V. Auwera, P. Varanasi, G. Wagner, The HITRAN 2004 molecular spectroscopic database, J. Quant. Spectrosc. Radiat. Trans. 96 (2005) 139–204.
[21] V.L. Kasyutich, P.A. Martin, R.J. Holdsworth, Mid-infrared laser absorption spectrometers based upon all-diode laser difference frequency generation and a room temperature quantum cascade laser for detection of CO, N_2O and NO, Appl. Phys. B 92 (2008) 271–279.
[22] Z. Abd Allah, D. Sawtell, V.L. Kasyutich, P.A. Martin, FTIR and QCL diagnostics of the decomposition of volatile organic compounds in an atmospheric pressure dielectric packed bed plasma reactor, J. Phys. Conf. Ser. 157 (2009) 012001.
[23] R. Schieder, C. Kramer, Optimization of heterodyne observations using Allan variance measurements, Astronom. Astrophy. 373 (2001) 746–756.
[24] V. Ossenkopf, The stability of spectroscopic instruments: a unified Allan variance computation scheme, Astronom. Astrophy. 479 (2008) 915–926.
[25] B. Tuzson, M.J. Zeeman, M.S. Zahniser, L. Emmenegger, Quantum cascade laser based spectrometer for in situ stable carbon dioxide isotope measurements, Infrared Phys. Technol. 51 (2008) 198–206.
[26] V.L. Kasyutich, P.A. Martin, R.J. Holdsworth, Phase-shift off-axis cavity-enhanced absorption detector of nitrogen dioxide, Meas. Sci. Technol. 17 (2006) 923–931.
[27] V.L. Kasyutich, C.E. Canosa-Mass, C. Pfrang, S. Vaughan, R.P. Wayne, Off-axis continuous-wave cavity-enhanced absorption spectroscopy of narrow-band and broad-band absorbers using red diode lasers, Appl. Phys. B 75 (2002) 755–761.
[28] Y.A. Bakhirkin, A.A. Kosterev, R.F. Curl, F.K. Tittel, D.A. Yarekha, L. Hvozdara, M. Giovannini, J. Faist, Sub-ppbv nitric oxide concentration measurements using cw thermoelectrically cooled quantum cascade laser-based integrated cavity output spectroscopy, Appl. Phys. B 82 (2006) 149–154.
[29] V.L. Kasyutich, Laser beam patterns of an optical cavity formed by two twisted cylindrical mirrors, Appl. Phys. B 96 (2009) 141–148.
[30] S.M. Cristescu, S.T. Persijn, S. Te Lintel Hekkert, F.J.M. Harren, Laser-based systems for trace gas detection in life sciences, Appl. Phys. B 92 (2008) 343–349.
[31] S.M. Chernin, Multipass matrix systems for diode laser spectroscope, Infrared Phys. Technol. 37 (1996) 87–93.

Please cite this article in press as: V.L. Kasyutich et al., Stability of widely tuneable, continuous wave external-cavity quantum cascade laser for absorption spectroscopy, Infrared Phys. Technol. (2010), doi:10.1016/j.infrared.2010.07.004